

Self-Powered Multifunctional Electronic Skin for a Smart Anti-Counterfeiting Signature System

Hang Guo, Ji Wan, Hanxiang Wu, Haobin Wang, Liming Miao, Yu Song, Haotian Chen, Mengdi Han,* and Haixia Zhang*



Cite This: *ACS Appl. Mater. Interfaces* 2020, 12, 22357–22364



Read Online

ACCESS |



Metrics & More



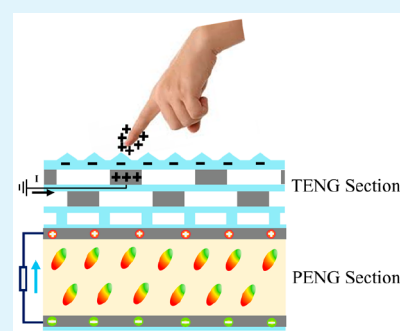
Article Recommendations



Supporting Information

ABSTRACT: Self-powered electronic skin is a promising field for human–machine interfaces to the next generation of intelligent and interactive products due to its capability of including multiple physical parameters for sensing without additional energy supply. This paper reports a novel active multifunctional electronic skin capable of independently detecting contact trajectory, acceleration, velocity, and pressure based on the synchronized triboelectrification and piezoelectric effect. Motion trajectories in the full plane can be identified by using a net-cross electrodes configuration design. Under this electrode special structure design, the motion information such as velocity and acceleration can be accurately obtained by the time difference between the peak values of the triboelectric signal. Real-time detection of dynamic pressure with only two electrodes is achieved by a spacer-grid design and a high quality piezoelectric nanofiber film. By virtue of its high sensitivity and precision, a smart anti-counterfeiting signature system (SASS) can be achieved by this self-powered multifunctional electronic skin with the capability of recognizing the writing habits of people within a 100 ms error for security. It is also a promising candidate in terms of human–machine interaction, cyber security, and so on.

KEYWORDS: self-powered, multifunctional electronic skin, PVDF–TrFE, triboelectric nanogenerator (TENG), smart anti-counterfeiting signature system (SASS)



1. INTRODUCTION

The fast progressing electronic skins are spreading their applications into many aspects of human life. Researchers have been applying intensive efforts to the construction of a solid and systematic study of multifunctional electronic skins^{1–5} due to their potential to integrate a variety of sensing capabilities,⁶ such as humidity,⁷ temperature,⁸ motion,^{9–11} and chemicals,¹² just like the skins do. Among all these functions, motion sensing is one of the most important ones for artificial intelligence^{13–17} because motion is a simple and efficient way for humans to interact with them. When focusing on the scope of motion sensing functions in electronic skins, a generally adopted approach can be summarized as developing pressure sensors first, then followed by integrating such units into digital arrays.^{18–21} However, certain drawbacks exist in this routine procedure. For example, to increase the resolution, the number of electrodes will increase in the N^2 mode; on the other hand, to be able to integrate pressure sensing detection, the small unit of each device is usually composed of piezoresistive or pressure capacity. In that way, resolution enhancement relies on an increased number of sensing units which leads to a huge number of electrodes, while frequent recharging of batteries is also inevitable. Both of the disadvantages severely hamper the feasibility of a portable electronic system featuring electronic skins. Nevertheless, self-powered systems^{22–33} and ingenious electrodes structure design point out potential solutions. The

self-powered systems harness the energy in the surrounding environment and thus provide the opportunity to get rid of batteries, while the ingenious electrodes structure design can achieve the $2N$ mode replacing the N^2 mode when increasing the resolution.

Herein, we report an active electronic skin device that enables real-time multifunctional motion detection. The self-powered electronic skin is composed of two sections (triboelectric nanogenerator (TENG) and piezoelectric nanogenerator (PENG)). When a moving object moves on the surface of the device, the motion information about the moving object can be simultaneously obtained by the triboelectrification and piezoelectric signals without external power supply based on the triboelectrification and piezoelectric effects in real time. In this way, the multifunctional electronic skin also as the SASS can recognize the pressure, velocity, pause time, trajectory, and corresponding sequences of the signatures. The system SASS can accurately recognize people's writing habits within the error range of a 100 ms; therefore, it

Received: February 23, 2020

Accepted: April 15, 2020

Published: April 15, 2020



has great application prospects in human–machine interaction and network security.

2. RESULTS AND DISCUSSION

Figure 1a shows a schematic view of the structure of the TENG section, which measures 8 cm by 8 cm. As can be seen

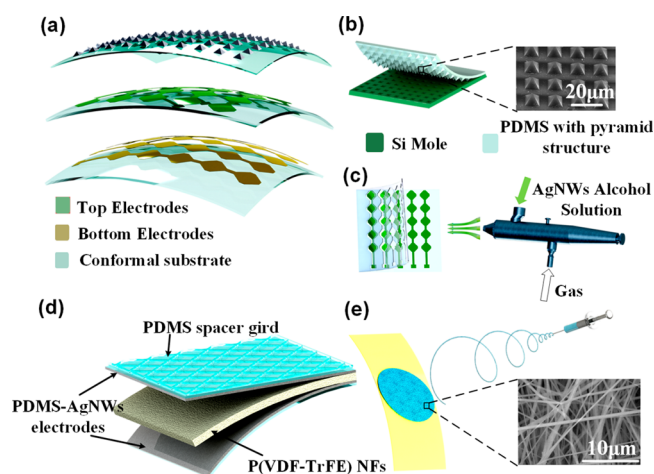


Figure 1. Structure and fabrication process of the electronic skin. (a) Schematic diagrams of the TENG sensor section. (b) PDMS film and SEM image of the inverted microstructure by the inverted pyramid microstructure. (c) Process for preparing AgNWs transparent electrodes by spraying on the PDMS substrate. (d) Schematic diagrams of the PENG sensor section including AgNWs electrodes on the PDMS substrate and PVDF–TrFE nanofibers (the top layer has a PDMS spacer network corresponding to the TENG section). (e) Fabrication process of PVDF–TrFE nanofibers by high-voltage electrospinning and the SEM image on the right.

from Figure 1a, the TENG portion consists of three layers of flexible film, with the topmost layer being a polydimethylsilane (PDMS) film with an inverted pyramid structure and the lower two layers being a patterned PDMS–silver nanowires (AgNWs) conductive film. The three layers of flexible film are bonded by uncured PDMS and then heat-cured to form a unit. Figure 1b,c details the preparation of a three-layer film. It is worth noting that the patterned PDMS–AgNWs film formed by spraying with a PI mask is carefully designed to include five parallel electrodes, and each electrode consists of five quadrilateral valves. When two layers of such patterned PDMS–AgNWs films are stacked vertically with each other, the two electrode patterns complement each other to form a crisscross network, which plays a very good role in track recognition and velocity. A PDMS film with a pyramid microstructure can be prepared by using a previously prepared silicon mold with inverted pyramids (where the SEM image is shown on the right side of Figure 1b). The microstructured PDMS film on the top layer can increase the triboelectric signals.

Figure 1d shows a schematic of the PENG section, from which it can be seen that PENG also uses the PDMS–AgNWs conductive film to make the overall device flexible. The PDMS–AgNWs electrode film is also sprayed but different from the TENG section. The PENG section conductive film does not use the PI mask during the spraying process, which can make the conductive AgNWs network be uniformly distributed over the entire plane. It is also advantageous for increasing the contact area between the electrode and the

piezoelectric layer and increasing the output piezoelectric signal. The core piezoelectric layer of PENG is a poly(vinylidene difluoride)–trifluoroethylene, PVDF–TrFE, piezoelectric copolymer prepared by high-voltage electrospinning. An SEM image of the electrospun PVDF–TrFE nanofibers is shown in Figure 1e.

The device is mainly composed of the TENG and PENG sections. It can be seen from the top view of the TENG section (Figure S1) that the device plane is divided into a quadrilateral array by the patterned electrodes. Correspondingly, we designed a spacer grid with respect to this quadrilateral array in the upper part of the PENG section. It can also be seen from the schematic cross-sectional view of the device (Figure S2) that the spacer grid just separates the quadrilateral array composed of patterned electrodes. The spacer grid is the key to dynamic pressure testing.

2.1. TENG Section. Figure 2a shows the working mechanism of the TENG component to generate a signal. When an object (such as a finger) touches the surface of device, a contact electrification phenomenon occurs. Because PDMS has a stronger ability to attract electrons, it usually has a negative charge on the surface of the PDMS, and the finger in contact with it has an opposite positive charge. It is this contact electrification process that provides a “signal source” for the entire device without the need for an external power supply.

As shown in Figure 2a(i), when a positively charged finger is about to slide to an electrode, the positive charge on the finger will gradually balance the negative charge on the PDMS surface. Therefore, at this time, there is a charge flowing from the electrode to the ground. When the finger moves to the electrode (Figure 2a(ii)), the electric field is confined between the surface of the finger and the surface of the PDMS. At this time, the voltage of the electrode will no longer be affected by the negative charge of the PDMS layer on the upper surface, and so there is no current generated in the electrical circuit. Then the finger leaves the electrode (Figure 2a(iii)), and the negative charge on the surface of the PDMS induces an opposite positive charge on the corresponding electrode due to the electrostatic induction effect. When the finger is completely drawn across one electrode and is approaching the next electrode (Figure 2a(iv)), similar to the previous process, there will be charge flowing from the electrode into the ground, and the above phenomenon will be repeated. Therefore, on the basis of the order and number of outputs of the electrical signals on each electrode, we can record the continuous sliding trajectory and motion state of the finger on the device. In addition, we can get the velocity and acceleration of the finger’s movement on the surface of the device.

Because the multifunctional electronic skin can detect the trajectory of the motion of the object by the order of the electrode signals, the trajectory detection characteristic is introduced here. With different motion trajectories, the order and period of the output signals will also change. In addition to the basic trajectory recognition (Figure S3), the device can also identify individual letters. Here we demonstrate the writing of the letters “P”, “K”, and “U” on the surface of the device (Figure 2b–d).

From the diagram on the left, we can observe that the letter can be decomposed into several unidirectional motion trajectories. We can find that the writing process of the letter “P” can be split into four tracks (Figure 2b). The first track is the motion along the three patterns on the electrode T1 and sequentially through the bottom electrodes B4, B3, and B2.

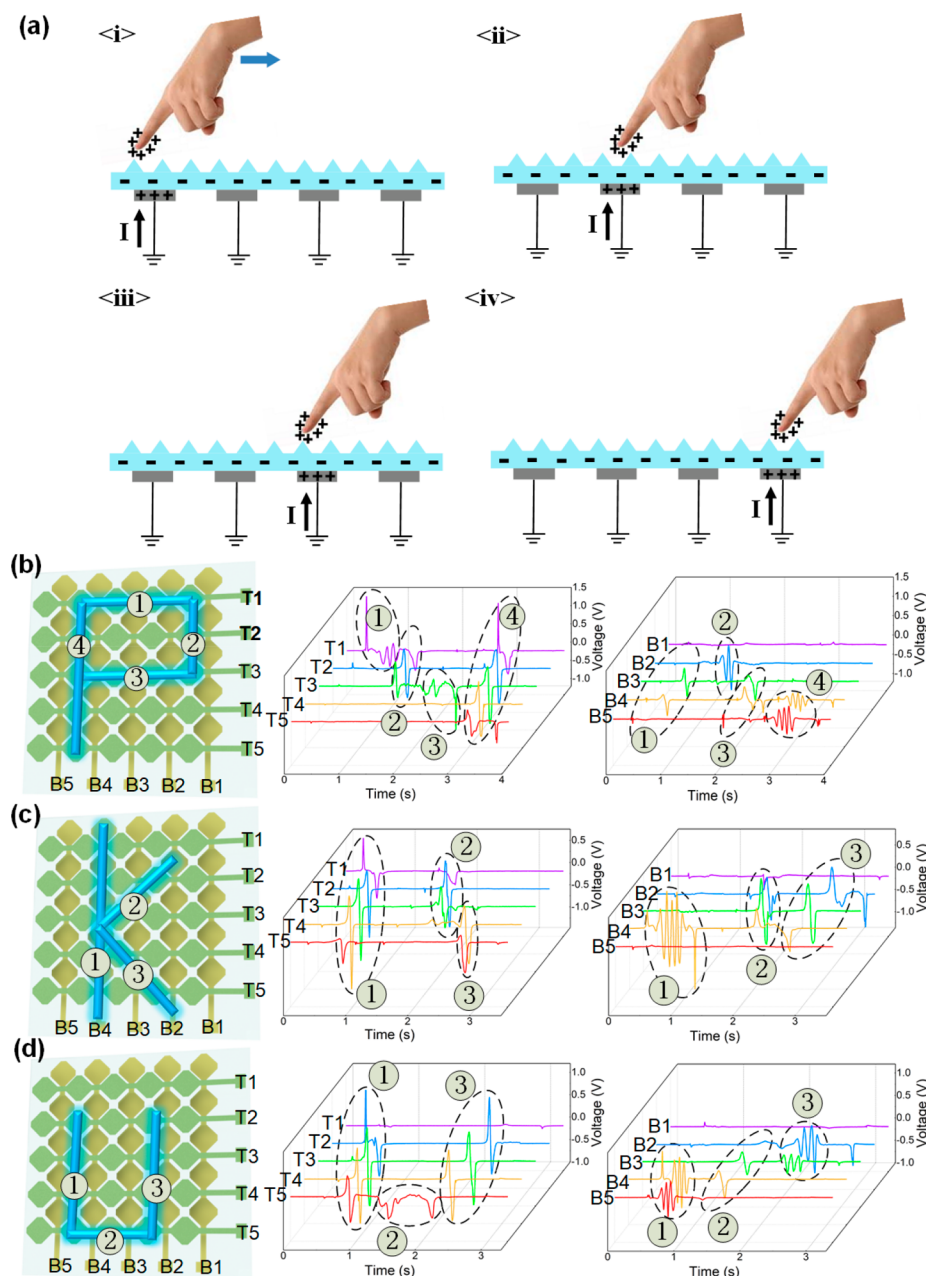


Figure 2. Illustration of the working principle of the electronic skin. (a) Trajectory detection principle based on triboelectrification and electrostatic induction. Write the track letters (b–d) “P”, “K”, and “U” on the surface of the device and triboelectric signals corresponding to the respective electrodes.

The second track is the longitudinal movement through the electrodes T1 and T2. The third track is along the electrode T3; the pattern of the three patterns passing through the bottom electrode is exactly opposite to the first track. The fourth track is the longitudinal movement through the electrodes B4 and B5. From the signal diagrams on the respective electrodes on the right of Figure 2b, we can well observe the electrode signal maps that correspond one-to-one with each trajectory. Similarly, we can also decompose the trajectory of the letter “K” into three motion trajectories. The first track is the motion along the bottom electrode B4. It can also be seen in the electrode signal diagram in Figure 2c that there are five signal peaks on the electrode B4. In addition, since the moving object sequentially passes through the electrodes T1 to T5, a signal peak is sequentially induced on

the electrodes T1 to T5. The second and third trajectories are both diagonally moving, so the main reaction in the signal diagram is to induce signal peaks on each electrode in turn. The movement of the letter “U” can also be divided into three trajectories (Figure 2d), the first of which is the longitudinal movement through the electrodes B4 and B5, thus inducing a continuously repeated signal peak on the electrodes B4 and B5, while T2 to T4 will also in turn induce signal peaks. The second trajectory is the motion along the electrode T5. The third trajectory is similar to the first one, but the position changes to the bottom electrodes B2 and B3.

In the above analysis, the device recognizes the motion trajectory by the number and sequence of the induced signal peaks on the electrodes and applies and recognizes each letter. In addition, since the structure of the device is such that the

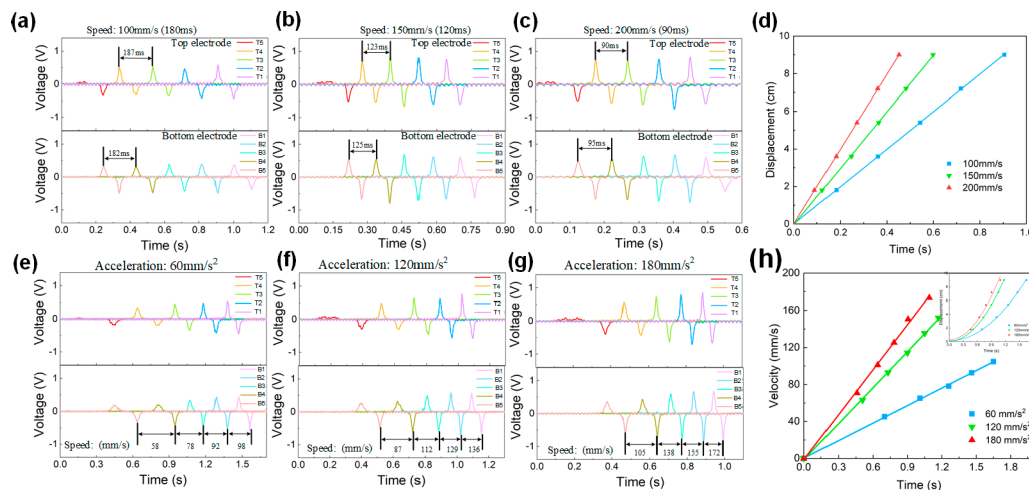


Figure 3. Detection velocity and acceleration. (a–c) Signals of the corresponding electrodes when swipe at a constant velocity across the surface of the device at different high velocities (100, 150, and 200 mm/s). (d) Detected displacement of the object over time and curve fitting. (e–g) Signals of the corresponding electrodes when accelerate sliding across the surface of the device at a constant acceleration (60, 120, and 180 mm/s²). (h) Detected velocity of the object over time and curve fitting. Inset is the fit of displacement over time.

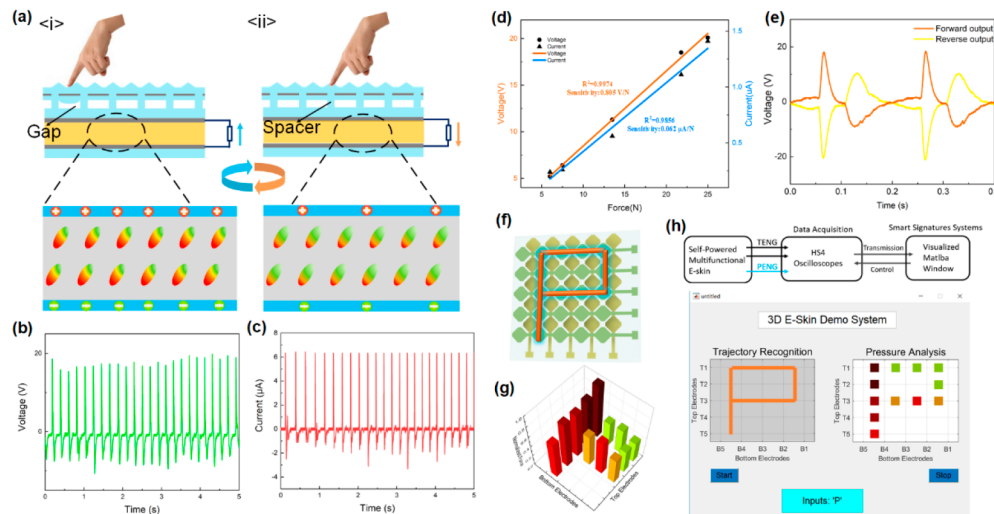


Figure 4. PENG section for detecting pressure in real time. (a) Illustration of the working principle of pressure based on piezoelectric effect. (b, c) Voltage and current output of the PENG section. (d) Linear fit of PENG section output to applied pressure. (e) Output of PENG film with forward and reverse connection. (f–h) Smart recognition of the real-time pressure of the letter “P” in the SASS.

upper and lower electrodes are vertically overlapped with each other, the distance between two adjacent patterns on the electrode is a determined constant (Figure S4). Obviously, we can calculate the velocity and acceleration of a moving object by analyzing the time difference of the generated signal peak. During the test, we used a linear motor platform to provide stable velocity or acceleration and set different velocities by adjusting the velocity of the motor to facilitate calibration of the device. During the test, the object is attached to the linear motor and follows a movement. By dividing the distance between two adjacent electrode patterns by the time difference corresponding to the signal peak, we can derive the velocity of the object motion. Figure 3a–c shows the time difference between the peaks of induced signals at each electrode during motion at different velocities (100, 150, and 200 mm/s). To demonstrate accurate measurement of sensing velocity and acceleration, we use the diagonal path during the test to obtain more electrical signal data. Figure 3d also shows the velocity measurement fit curves at different velocities. Figure 3e–h

shows the time interval of the induced electrical signal peaks at each electrode and the acceleration measurement fit at different accelerations (60, 120, and 180 mm/s²).

2.2. PENG Section. Figure 4a shows the working mechanism of PENG-induced pressure. Piezoelectric film-based PENG has two working mechanisms: a pressure applied (d33) mode and a curved (d31) mode. When measuring pressure in real time with multifunctional electronic skin, we used the d33 mode of the PVDF–TrFE piezoelectric film. PENG works differently from TENG, which generates an electrical signal only during the deformation–recovery process. Because of TENG’s electrode structure design, in this work, we designed a spacer network corresponding to the TENG partial electrode pattern on top of PENG to accommodate PENG’s d33 mode. The linear increase of output for the PENG can be derived from the equation $V_{OC} = T\delta_{33}g_{33}$, where T is the thickness of the piezoelectric material, δ_{33} is the stress along the direction of the applied force, and g_{33} is the piezoelectric voltage coefficient. Because the thickness of PDMS will affect

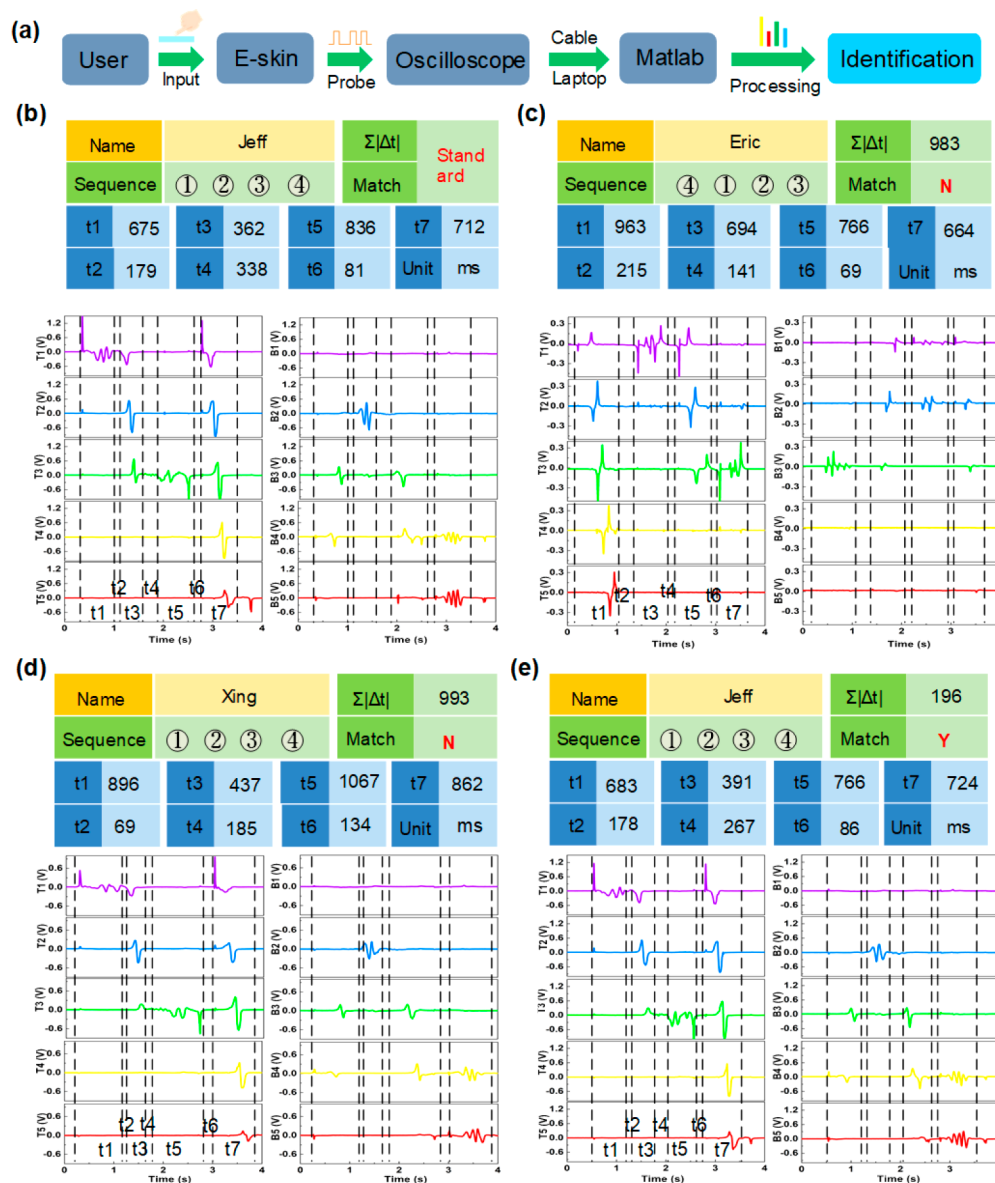


Figure 5. (a) SASS as a human–computer interaction interface to recognize the people’s writing habits for security and smart anti-counterfeiting. (b) Standard signals of “Jeff” when signing. (c–e) Signals of “Eric”, “Xing”, and “Jeff” when signing the same track.

the size of δ_{33} , $\delta_{33} = F/S$, where F is the applied pressure and S is the cross-sectional area of PDMS. Because of the existence of the above-mentioned spacer grid structure, the cross-sectional area of the device at the spacer is larger than that of the gap. That is, the polarization intensity of the crystal in the piezoelectric film is different when the pressure that is applied moves to the spacer and the gap (shown in Figure 4a), so the device can dynamically respond to the pressure. When the object slides on the surface of the device, it will continuously pass through the spacer and the gap. Therefore, the cross-sectional area S is the changing value. Therefore, V_{OC} also changes with the passing position of the object. In the loop, the current is constantly generated in the opposite direction. As shown in Figure 4, when the object moves to the gap, V_{OC} becomes larger because of S decrease, and when the object moves to the spacer, V_{OC} decreases because of S increase.

Figure 4b,c shows open-circuit voltage and short-circuit current, and Figure 4e shows output of the PENG film with forward and reverse connection. In summary, when the finger

slides on the surface of the device, the PVDF–TrFE piezoelectric nanofiber membrane sensing the dynamic pressure can sense the finger pressure in the sliding state due to the existence of a specially designed spacer network.

To research the pressure sensing of the PENG module in the multifunctional electronic skin, we applied different pressures from 6 to 25 N and measured the output voltage and current of PENG for different pressures. Figure 4d shows the linear fit of the piezoelectric film voltage and current output to the pressure. By fitting the curve, we can see that the voltage output fitting degree R^2 reached 0.9974, and the current output fitting degree R^2 also reached 0.9856. This result also shows that the PVDF–TrFE prepared by high-voltage electrostatic spinning nanofibers has very good piezoelectric properties. By calculation, the voltage and current sensitivity of the PENG part reached 0.805 V/N and 0.062 μ A/N, respectively.

On this basis, as shown in Figure 4f–h, we apply a time-varying pressure in the SASS to write the letter “P”. A total of 12 electrodes are connected to probes from three HS4

oscilloscopes for data acquisition, with 10 electrodes in the TENG section and two electrodes in the PENG section. The oscilloscope's measurements can be controlled by the computer, and the signal extraction information can be obtained directly. Figure 4g shows the magnitude of the pressure as it passes through each pad portion in normalization. In the SASS, trajectories and real-time normalized pressure are identified in Figure 4h. The track signal from TENG obtained by the Matlab program can be used to identify the input letters. By normalizing the pressure signal from PENG, one can feel the pressure used in the process of writing letters in real time.

To explain that when the finger slides on the surface of the multifunctional electronic device, the triboelectric charge generated by the upper layer TENG does not interfere with the PENG of the lower layer. Here, we elaborate on two aspects: Because the influence of electrostatic induction decreases exponentially with increasing distance, we can observe that there is a small amount of triboelectric charge near the surface of the piezoelectric material. Therefore, in terms of the amount of charge, the triboelectric charge here does not affect the piezoelectric effect. On the other hand, because of our special structural design, the upper and lower patterned electrodes of the piezoelectric film are in the same shape as the spacer network. The gasket network is complementary to the triboelectric generator electrodes. Therefore, from the time domain perspective, the triboelectric signal and the piezoelectric signal do not appear at the same time, but alternately appear, so they do not affect each other.

2.3. Applications. Finally, a demonstration of the practical usage of the self-powered multifunctional electronic skin as a smart anti-counterfeiting signature system (SASS) is performed, in which the device also serves as a human-machine interface. Figure 5 shows the system for smart anti-counterfeiting signature. The signature is a valid identifier for the current authentication system, but the inability to accurately identify signature features (trajectory, velocity, pause time, etc.) poses significant challenges to security and numerous information security issues. Here, on the basis of the SASS system, we have performed accurate intelligent signature recognition and anti-counterfeiting authentication for personal writing habits that are not recognized by the traditional anti-counterfeiting mode.

Figure 5b shows the signal analysis of four groups of signatures written by three students (Jeff, Eric, and Xing) in the SASS system. They signed the trajectory of the letter "P" on the multifunctional electronic skin in their own habits. Here we set Jeff's first signature signals as standard. From the TENG section above, we can already get a written path from the system divided into four tracks. Therefore, we divide the entire trajectory process into seven time periods (t_1-t_7) according to the track. In the signal diagram, we can see that Eric's writing path is different from the standard path. The difference between the time spent by Xing and the standard is large. For quantitative representation, we compare each path time period with a standard time period (Δt_i). After the signatures of Jeff, Eric, and Xing are compared with the standard signature, $\sum|\Delta t_{\text{Eric}}| = 983$ ms, $\sum|\Delta t_{\text{Xing}}| = 993$ ms, and $\sum|\Delta t_{\text{Jeff}}| = 196$ ms. We can set a threshold $\sum|\Delta t_i| = 500$ ms; one can see that Jeff's signature signal is far below the set threshold, and Xing and Eric's signature signals are much larger than the threshold, indicating that the SASS system has accurate anti-counterfeiting identification.

3. CONCLUSION

In conclusion, we have prepared a self-powered multifunctional electronic skin integrating motion tracking, velocity, acceleration, pressure, and other physical information detection. A smart anti-counterfeiting signature system (SASS) is developed based on the electronic skin as a human-computer interaction interface to identify the personal signature habits of users and realize anti-counterfeiting. The SASS utilizes triboelectric and piezoelectric signals for sensing, so that there is no need for external energy supply. Accurate trajectory and velocity sensing are achieved by using a special electrode structure design with vertical cross-stacking. The dynamic pressure is detected by a spacers-cavity structure. In terms of the fabrication process, patterned electrodes and high-quality piezoelectric nanofiber films were obtained by using an AgNWs spraying process and an electrospinning process. In addition, the patterned silver nanowire AgNWs electrodes are sprayed onto the PDMS substrate to achieve good transparency and stretchability. This self-powered multifunctional electronic skin demonstrates its great application prospects in the human-computer interaction interface and intelligent recognition.

4. MATERIALS AND METHODS

4.1. Fabrication of Patterned PDMS-AgNWs Thin Film.

First, the PDMS base solution and the cross-linker (Sylgard 184, Dow Corning) were mixed uniformly at a mass ratio of 10:1 and evacuated for 20 min until the air bubbles were no longer visible. The solution was dropped on the smooth glass surface, spin-coated at 1200 rpm for 80 s, and then heated on the hot plate at 85 °C for 60 min to solidify. Then a polyimide (PI) mask prepared by laser cutting was placed onto the surface of the PDMS, and oxygen plasma treatment was performed to make the surface of PDMS film hydrophilic by Corona (Electro-Technic Products, Inc., USA). After repeatedly spray-coating an ethanol solution of AgNWs, the membrane was annealed at 100 °C for 10 min to enhance the conductivity and stability. Finally, the PI mask and patterned PDMS-AgNWs film were carefully peeled off sequentially.

In the above process, a complete PDMS-AgNWs film can be obtained without using a polyimide (PI) mask. The complete PDMS-AgNWs conductive film can be used as an electrode for PENG to sense and collect electrical signals generated by PVDF-TrFE piezoelectric films.

4.2. Fabrication of TENG Sensing Section. We coated the solution of PDMS on the Si mold with pyramid structure, spin-coated at 600 rpm for 100 s, and then heated on the hot plate at 85 °C for 60 min. After being peeled off carefully, the microstructured PDMS film with pyramid arrays was obtained as the top layer to enhance the triboelectrification signal, and the thickness of this layer was about 150 μm . Two PDMS-AgNWs films obtained from section 4.1 were stacked perpendicularly while vertically connected by liquid PDMS and then heated on the hot plate at 90 °C for 20 min. At last, the device was encapsulated with liquid PDMS and then cured to protect the AgNWs exposed. The overall thickness of the electronic skin was about 500 μm .

4.3. Fabrication of PENG Sensing Section. First, the PVDF-TrFE composites solution was prepared by dissolving PVDF-TrFE powder (Solvay, 75/25 wt %) into a mixture of dimethylformamide (DMF) and acetone with a ratio of 2:3 at the concentration of 14%. After stirring with a magnetic spinner for 4 h, electrospinning was performed to create a piezoelectric membrane. This was done by using copper foil as a collector at 15 kV, a flow rate of 1 mL/h, and a tip-collector distance of 10 cm. After evaporation of any remaining solvent, the resultant electrospun fiber mat was annealed at the temperature of 80 °C for 2 h and then polarized at the voltage of 5 kV with a distance of hundreds of micrometers to help the PVDF-TrFE transform to β -phase and further enhance the piezoelectric performance.

The PENG portion was a sandwich structure composed of a PVDF–TrFE piezoelectric film and two layers of a complete PDMS–AgNWs conductive film in section 4.1. Because of the dynamic pressure signal induced by the PVDF–TrFE piezoelectric film, a spacer network corresponding to the TENG pattern was prepared on top of the PENG.

4.4. Testing Method to Realize Quantitative Noncontact Motions. The output current of the device was measured by a low noise current preamplifier (Stanford Research SR570), and all the signals were recorded and displayed through a digital oscilloscope (Agilent DSO-X 2014A).

■ ASSOCIATED CONTENT

Supporting Information

The Supporting Information is available free of charge at <https://pubs.acs.org/doi/10.1021/acsami.0c03510>.

Figures S1–S4 (PDF)

■ AUTHOR INFORMATION

Corresponding Authors

Mengdi Han – Center for Bio-Integrated Electronics, Northwestern University, Evanston, Illinois 60208, United States; Email: hanmd1990@gmail.com

Haixia Zhang – Academy for Advanced Interdisciplinary Studies and National Key Laboratory of Science and Technology on Micro/Nano Fabrication, Peking University, Beijing 100871, China; Email: zhang-alice@pku.edu.cn

Authors

Hang Guo – Academy for Advanced Interdisciplinary Studies, Peking University, Beijing 100871, China; orcid.org/0000-0003-0933-9011

Ji Wan – National Key Laboratory of Science and Technology on Micro/Nano Fabrication, Peking University, Beijing 100871, China

Hanxiang Wu – National Key Laboratory of Science and Technology on Micro/Nano Fabrication, Peking University, Beijing 100871, China; orcid.org/0000-0002-8556-8468

Haobin Wang – National Key Laboratory of Science and Technology on Micro/Nano Fabrication, Peking University, Beijing 100871, China

Liming Miao – National Key Laboratory of Science and Technology on Micro/Nano Fabrication, Peking University, Beijing 100871, China

Yu Song – National Key Laboratory of Science and Technology on Micro/Nano Fabrication, Peking University, Beijing 100871, China; orcid.org/0000-0002-4185-2256

Haotian Chen – Academy for Advanced Interdisciplinary Studies, Peking University, Beijing 100871, China

Complete contact information is available at: <https://pubs.acs.org/doi/10.1021/acsami.0c03510>

Notes

The authors declare no competing financial interest.

■ ACKNOWLEDGMENTS

This work was supported by the National Key R&D Project from the Ministry of Science and Technology, China (2018YFA0108100, 2016YFA0202701), and the National Natural Science Foundation of China (Grant No. 61674004).

■ REFERENCES

- (1) Chortos, A.; Liu, J.; Bao, Z. Pursuing Prosthetic Electronic Skin. *Nat. Mater.* **2016**, *15* (9), 937.
- (2) Chen, H.; Song, Y.; Cheng, X.; Zhang, H. Self-Powered Electronic Skin Based on the Triboelectric Generator. *Nano Energy* **2019**, *56*, 252–268.
- (3) Shi, Q.; He, T.; Lee, C. More than Energy Harvesting—Combining Triboelectric Nanogenerator and Flexible Electronics Technology for Enabling Novel Micro-/Nano-Systems. *Nano Energy* **2019**, *57*, 851–871.
- (4) Wang, X.; Dong, L.; Zhang, H.; Yu, R.; Pan, C.; Wang, Z. L. Recent Progress in Electronic Skin. *Advanced Science* **2015**, *2* (10), 1500169.
- (5) Hammock, M. L.; Chortos, A.; Tee, B. C. K.; Tok, J. B. H.; Bao, Z. 25th Anniversary Article: The Evolution of Electronic Skin (E-Skin): A Brief History, Design Considerations, and Recent Progress. *Adv. Mater.* **2013**, *25* (42), 5997–6038.
- (6) Park, M.; Park, Y. J.; Chen, X.; Park, Y. K.; Kim, M. S.; Ahn, J. H. Mos2-Based Tactile Sensor for Electronic Skin Applications. *Adv. Mater.* **2016**, *28* (13), 2556–2562.
- (7) Ho, D. H.; Sun, Q.; Kim, S. Y.; Han, J. T.; Kim, D. H.; Cho, J. H. Stretchable and Multimodal All Graphene Electronic Skin. *Adv. Mater.* **2016**, *28* (13), 2601–2608.
- (8) Trung, T. Q.; Ramasundaram, S.; Hwang, B. U.; Lee, N. E. An All-Elastomeric Transparent and Stretchable Temperature Sensor for Body-Attachable Wearable Electronics. *Adv. Mater.* **2016**, *28* (3), 502–509.
- (9) Guo, H.; Wu, H.; Song, Y.; Miao, L.; Chen, X.; Chen, H.; Su, Z.; Han, M.; Zhang, H. Self-Powered Digital-Analog Hybrid Electronic Skin for Noncontact Displacement Sensing. *Nano Energy* **2019**, *58*, 121–129.
- (10) Guo, H.; Chen, X. X.; Wu, H. X.; Song, Y.; Chen, H. T.; Zhang, H. X. Stretchable Location Sensor Based on Transparent AgNWs Electrodes. *2018 IEEE 13th Annual International Conference on Nano/Micro Engineered and Molecular Systems (NEMS)*; IEEE: 2018; pp 373–376.
- (11) Guo, H.; Chen, X.; Miao, L.; Wang, H.; Wan, J.; Zhang, H. Self-Powered Transparent Stretchable 3D Motion Sensor. *2019 20th International Conference on Solid-State Sensors, Actuators and Microsystems & Eurosensors XXXIII (TRANSDUCERS & EUROSENSORS XXXIII)*; IEEE: 2019; pp 554–557.
- (12) Yang, Y.; Gao, W. Wearable and Flexible Electronics for Continuous Molecular Monitoring. *Chem. Soc. Rev.* **2019**, *48* (6), 1465–1491.
- (13) Wang, X.; Zhang, H.; Dong, L.; Han, X.; Du, W.; Zhai, J.; Pan, C.; Wang, Z. L. Self-Powered High-Resolution and Pressure-Sensitive Triboelectric Sensor Matrix for Real-Time Tactile Mapping. *Adv. Mater.* **2016**, *28* (15), 2896–2903.
- (14) Wei, X. Y.; Wang, X.; Kuang, S. Y.; Su, L.; Li, H. Y.; Wang, Y.; Pan, C.; Wang, Z. L.; Zhu, G. Dynamic Triboelectrification-Induced Electroluminescence and Its Use in Visualized Sensing. *Adv. Mater.* **2016**, *28* (31), 6656–6664.
- (15) Yang, Z. W.; Pang, Y.; Zhang, L.; Lu, C.; Chen, J.; Zhou, T.; Zhang, C.; Wang, Z. L. Tribotronic Transistor Array as an Active Tactile Sensing System. *ACS Nano* **2016**, *10* (12), 10912–10920.
- (16) Wang, X.; Zhang, Y.; Zhang, X.; Huo, Z.; Li, X.; Que, M.; Peng, Z.; Wang, H.; Pan, C. A Highly Stretchable Transparent Self-Powered Triboelectric Tactile Sensor with Metallized Nanofibers for Wearable Electronics. *Adv. Mater.* **2018**, *30* (12), 1706738.
- (17) Chen, T.; Shi, Q.; Zhu, M.; He, T.; Sun, L.; Yang, L.; Lee, C. Triboelectric Self-Powered Wearable Flexible Patch as 3D Motion Control Interface for Robotic Manipulator. *ACS Nano* **2018**, *12* (11), 11561–11571.
- (18) Meng, Y.; Zhao, J.; Yang, X.; Zhao, C.; Qin, S.; Cho, J. H.; Zhang, C.; Sun, Q.; Wang, Z. L. Mechanosensation-Active Matrix Based on Direct-Contact Tribotronic Planar Graphene Transistor Array. *ACS Nano* **2018**, *12* (9), 9381–9389.
- (19) Zhang, Q.; Jiang, T.; Ho, D.; Qin, S.; Yang, X.; Cho, J. H.; Sun, Q.; Wang, Z. L. Transparent and Self-Powered Multistage Sensation

Matrix for Mechanosensation Application. *ACS Nano* **2018**, *12* (1), 254–262.

(20) Sun, Q.; Kim, D. H.; Park, S. S.; Lee, N. Y.; Zhang, Y.; Lee, J. H.; Cho, K.; Cho, J. H. Transparent, Low-Power Pressure Sensor Matrix Based on Coplanar-Gate Graphene Transistors. *Adv. Mater.* **2014**, *26* (27), 4735–4740.

(21) Sun, Q.; Seung, W.; Kim, B. J.; Seo, S.; Kim, S. W.; Cho, J. H. Active Matrix Electronic Skin Strain Sensor Based on Piezopotential-Powered Graphene Transistors. *Adv. Mater.* **2015**, *27* (22), 3411–3417.

(22) Hu, X.; Yan, X.; Gong, L.; Wang, F.; Xu, Y.; Feng, L.; Zhang, D.; Jiang, Y. Improved Piezoelectric Sensing Performance of P(VDF-TrFE) Nanofibers by Utilizing BTO Nanoparticles and Penetrated Electrodes. *ACS Appl. Mater. Interfaces* **2019**, *11* (7), 7379–7386.

(23) Jeong, C. K.; Baek, C.; Kingon, A. I.; Park, K. I.; Kim, S. H. Lead-Free Perovskite Nanowire-Employed Piezopolymer for Highly Efficient Flexible Nanocomposite Energy Harvester. *Small* **2018**, *14* (19), 1704022.

(24) Song, Y.; Zhang, J.; Guo, H.; Chen, X.; Su, Z.; Chen, H.; Cheng, X.; Zhang, H. All-Fabric-Based Wearable Self-Charging Power Cloth. *Appl. Phys. Lett.* **2017**, *111* (7), 073901.

(25) Chen, H.; Song, Y.; Guo, H.; Miao, L.; Chen, X.; Su, Z.; Zhang, H. Hybrid Porous Micro Structured Finger Skin Inspired Self-Powered Electronic Skin System for Pressure Sensing And Sliding Detection. *Nano Energy* **2018**, *51*, 496–503.

(26) Wu, H.; Guo, H.; Su, Z.; Shi, M.; Chen, X.; Cheng, X.; Han, M.; Zhang, H. Fabric-Based Self-Powered Noncontact Smart Gloves for Gesture Recognition. *J. Mater. Chem. A* **2018**, *6* (41), 20277–20288.

(27) Song, Y.; Wang, H.; Cheng, X.; Li, G.; Chen, X.; Chen, H.; Miao, L.; Zhang, X.; Zhang, H. High-Efficiency Self-Charging Smart Bracelet for Portable Electronics. *Nano Energy* **2019**, *55*, 29–36.

(28) Chen, X.; Guo, H.; Wu, H.; Chen, H.; Song, Y.; Su, Z.; Zhang, H. Hybrid Generator Based on Freestanding Magnet as All-Direction In-Plane Energy Harvester and Vibration Sensor. *Nano Energy* **2018**, *49*, 51–58.

(29) Wu, H.; Su, Z.; Shi, M.; Miao, L.; Song, Y.; Chen, H.; Han, M.; Zhang, H. Self-Powered Noncontact Electronic Skin for Motion Sensing. *Adv. Funct. Mater.* **2018**, *28* (6), 1704641.

(30) Chen, X.; Miao, L.; Guo, H.; Chen, H.; Song, Y.; Su, Z.; Zhang, H. Waterproof and Stretchable Triboelectric Nanogenerator for Biomechanical Energy Harvesting and Self-Powered Sensing. *Appl. Phys. Lett.* **2018**, *112* (20), 203902.

(31) Su, Z.; Wu, H.; Chen, H.; Guo, H.; Cheng, X.; Song, Y.; Chen, X.; Zhang, H. Digitalized Self-Powered Strain Gauge for Static and Dynamic Measurement. *Nano Energy* **2017**, *42*, 129–137.

(32) Zhang, J.; Song, Z.; Guo, H.; Song, Y.; Yu, B.; Zhang, H. GPS-Inspired Stretchable Self-Powered Electronic Skin. *IEEE Trans. Nanotechnol.* **2018**, *17* (3), 460–466.

(33) Shi, M.; Zhang, J.; Chen, H.; Han, M.; Shankaregowda, S. A.; Su, Z.; Meng, B.; Cheng, X.; Zhang, H. Self-Powered Analogue Smart Skin. *ACS Nano* **2016**, *10* (4), 4083–4091.